Supporting Information (Online Material) for

$Gd_2CuZnMn_4O_{12}$: A-site columnar-ordered perovskite with anisotropic thermal expansion and a gradual charge-order transition

Alexei A. Belik*

Research Center for Materials Nanoarchitectonics (MANA), National Institute for Materials Science (NIMS), Namiki 1-1, Tsukuba, Ibaraki 305-0044, Japan

E-mail: Alexei.Belik@nims.go.jp

Table S1. Selected Bond Lengths (l (Å) < 2.8 Å), Bond Angles (deg), Bond Valence Sums, BVS, and Distortion Parameters of MnO_6, Δ, in $Gd_2CuZnMn_4O_{12}$ at T = 100 K [a]

Gd1–O5 ×2	2.324(9)	Gd2–O2 ×2	2.361(9)
Gd1–O3 ×2	2.400(8)	Gd2–O4 ×2	2.377(9)
Gd1–O2 ×2	2.432(9)	Gd2–O5 ×2	2.424(9)
Gd1–O1 ×4	2.648(6)	Gd2–O1 ×4	2.659(6)
BVS($Gd1^{3+}$)	3.37	BVS($Gd2^{3+}$)	3.32
Cu–O1 ×4	1.958(4)	Zn–O4 ×2	1.997(9)
BVS(Cu^{2+})	1.88	Zn–O3 ×2	2.003(9)
		BVS(Zn^{2+})	1.80
Mn1–O2 ×2	1.890(2)	Mn2–O5 ×2	1.896(2)
Mn1–O3 ×2	1.944(3)	Mn2–O1 ×2	1.945(7)
Mn1–O1 ×2	2.159(7)	Mn2–O4 ×2	1.964(4)
BVS($Mn1^{3+}$)	3.30	BVS($Mn2^{4+}$)	3.68
Δ(Mn1–O)	33.8×10^{-4}	Δ(Mn2–O)	2.2×10^{-4}
Mn1–O1–Mn2 ×2	145.16(9)	Mn2–O4–Mn2	135.68(9)
Mn1–O2–Mn1	148.46(9)	Mn2–O5–Mn2	146.58(9)
Mn1–O3–Mn1	138.17(9)		

[a] BVS = $\sum_{i=1}^{N} v_i$, $v_i = \exp[(R_0 - l_i)/B]$, N is the coordination number, B = 0.37, $R_0(Gd^{3+})$ = 2.065, $R_0(Cu^{2+})$ = 1.679, $R_0(Zn^{2+})$ = 1.704, $R_0(Mn^{4+})$ = 1.753, and $R_0(Mn^{3+})$ = 1.76.

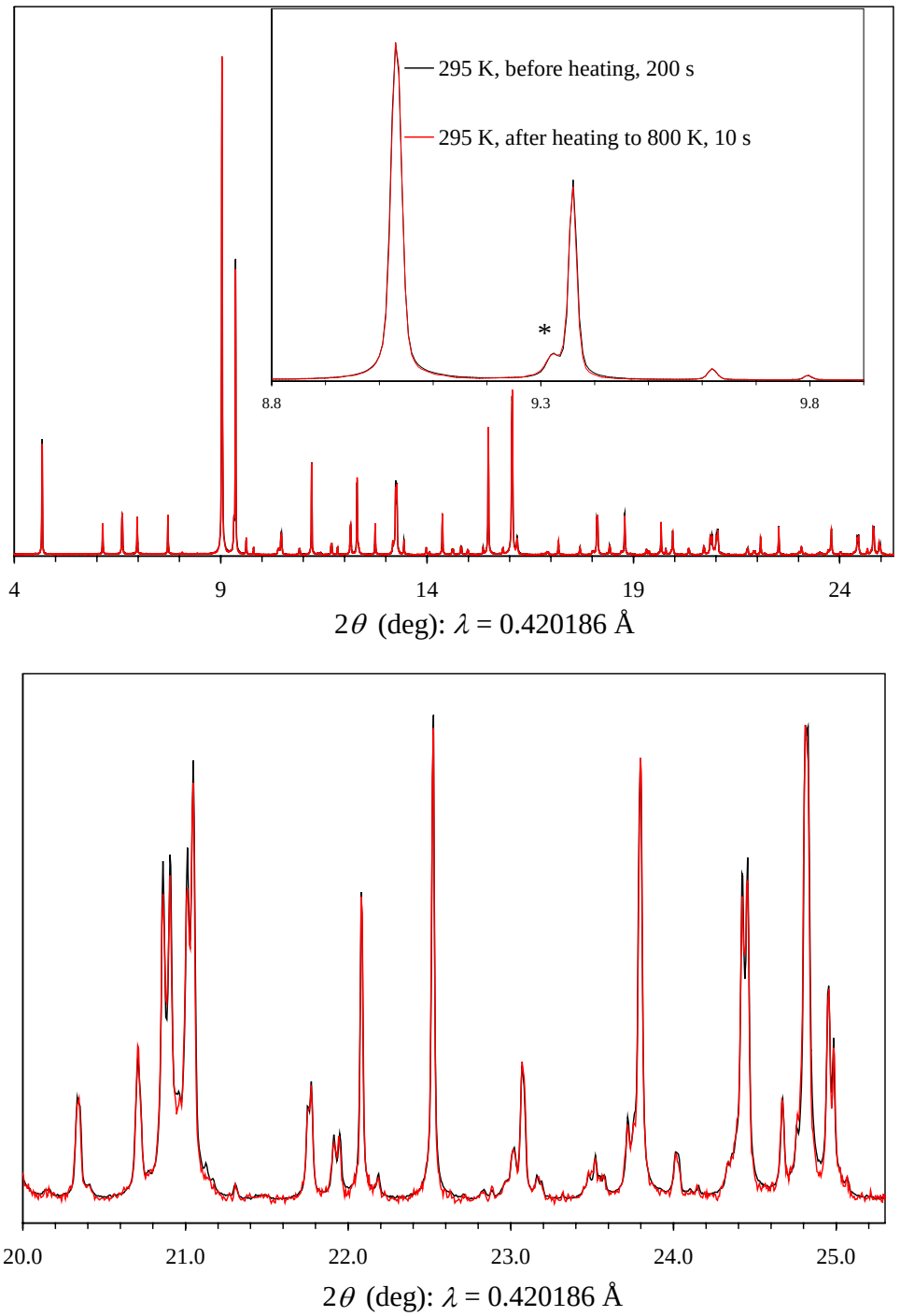

Figure S1. Fragments of (normalized) experimental synchrotron X-ray powder diffraction patterns of $Gd_2CuZnMn_4O_{12}$ at room temperature: the as-synthesized sample (the black curve) and a sample after heating to 800 K in high-temperature synchrotron X-ray powder diffraction experiments (the red curve). The star shows a contribution of the impurity.

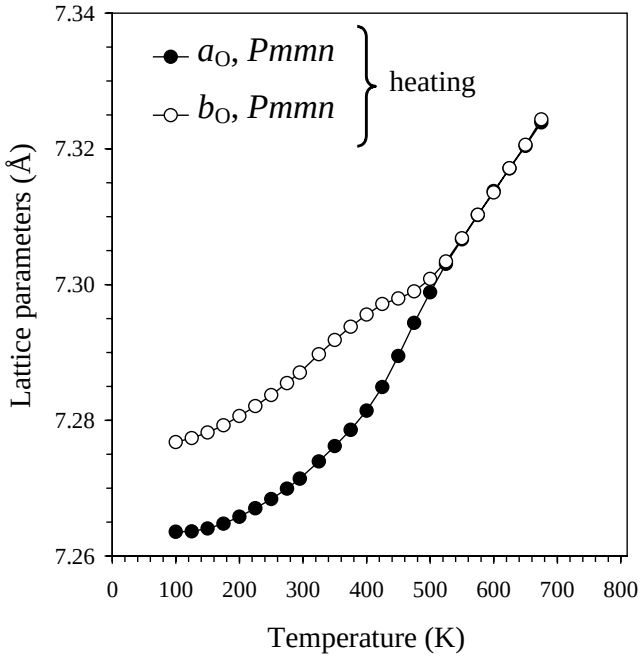

Figure S2a. Temperature dependence of the a_O and b_O lattice parameters of $Gd_2CuZnMn_4O_{12}$ between 100 K and 675 K on heating. The fitting at all these temperatures was performed in the *Pmmn* model.

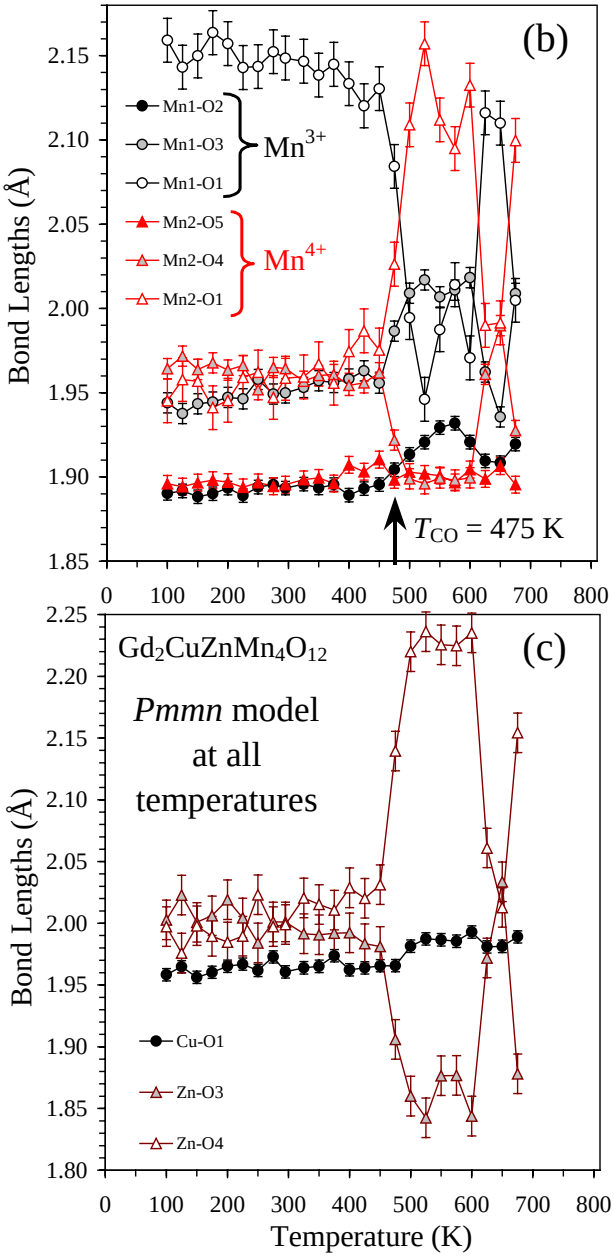

Figure S2b, 2c. Temperature dependence of (b) the Mn-O bond lengths and (c) the Cu-O and Zn-O bond lengths in $Gd_2CuZnMn_4O_{12}$ from 100 K to 675 K. The bond lengths were obtained in the *Pmmn* model. This figure illustrates that the refinement in the *Pmmn* model above T_{CO} gave unstable and correlated results giving evidence that the symmetry is higher.

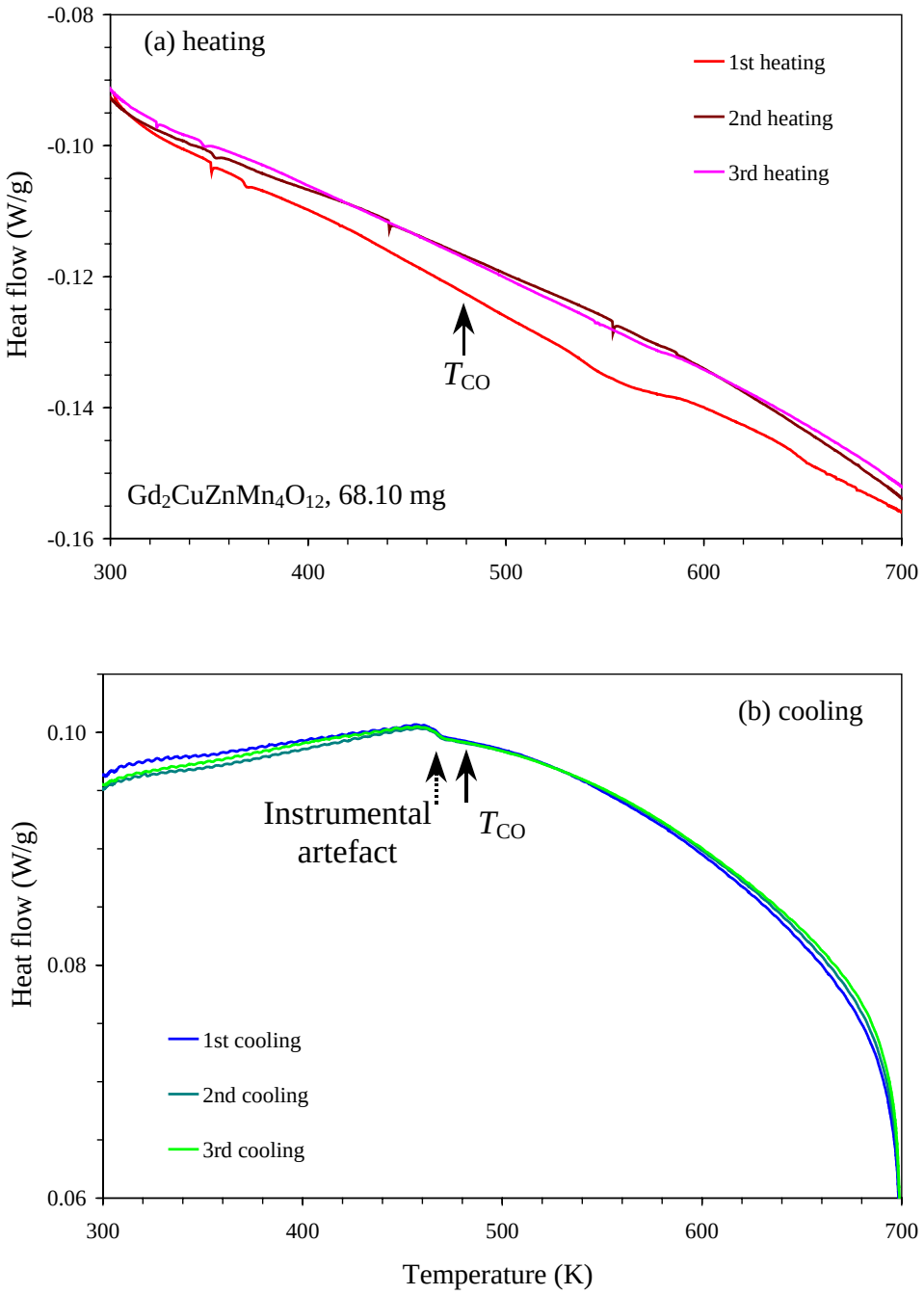

Figure S3. Differential scanning calorimetry (DSC) curves of a powder sample of $Gd_2CuZnMn_4O_{12}$ (68.10 mg) on (a) heating and (b) cooling. Three runs were performed to check the reproducibility. The (full) arrows show the charge-order phase transition temperature determined by high-temperature synchrotron X-ray powder diffraction – no anomalies were detected at this temperature by DSC. The dotted arrow shows anomalies from an instrument observed on nearly all measurements.

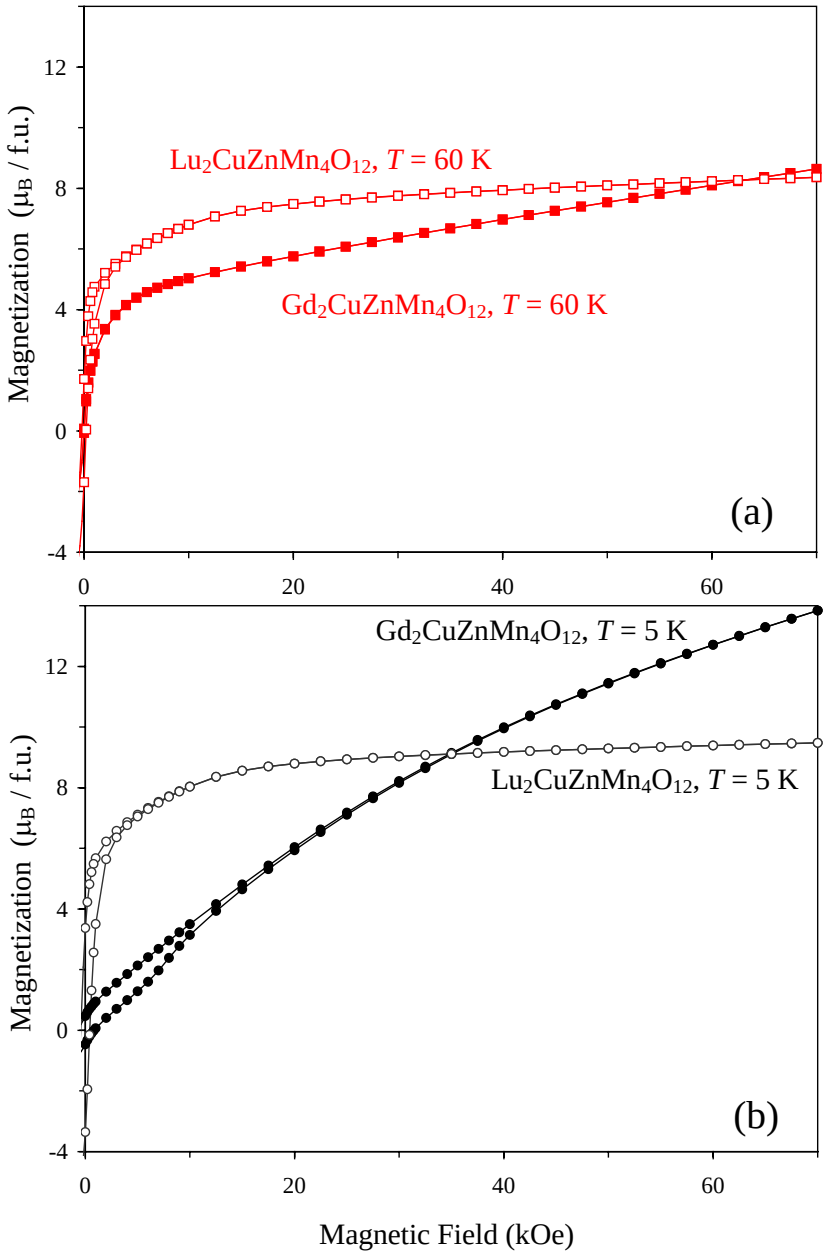

Figure S4. (a) *M* versus *H* curves of $Gd_2CuZnMn_4O_{12}$ in comparison with those of $Lu_2CuZnMn_4O_{12}$ (without magnetic rare-earth elements) at *T* = 60 K. The curves were quantitatively similar with small differences: $Lu_2CuZnMn_4O_{12}$ shows a saturated behavior typical for ferrimagnets while $Gd_2CuZnMn_4O_{12}$ shows a small linear increase of *M* with *H* (above about 10 kOe), probably due to paramagnetic contribution from the Gd sublattice. We can suggest a similar ferrimagnetic order between the Mn and Cu sublattices in these two compounds.
(b) *M* versus *H* curves of $Gd_2CuZnMn_4O_{12}$ in comparison with those of $Lu_2CuZnMn_4O_{12}$ at *T* = 5 K. The curves were quantitatively different. $Lu_2CuZnMn_4O_{12}$ still shows a saturated behavior typical for ferrimagnets while $Gd_2CuZnMn_4O_{12}$ shows a different behavior originating from the Gd sublattice contribution.

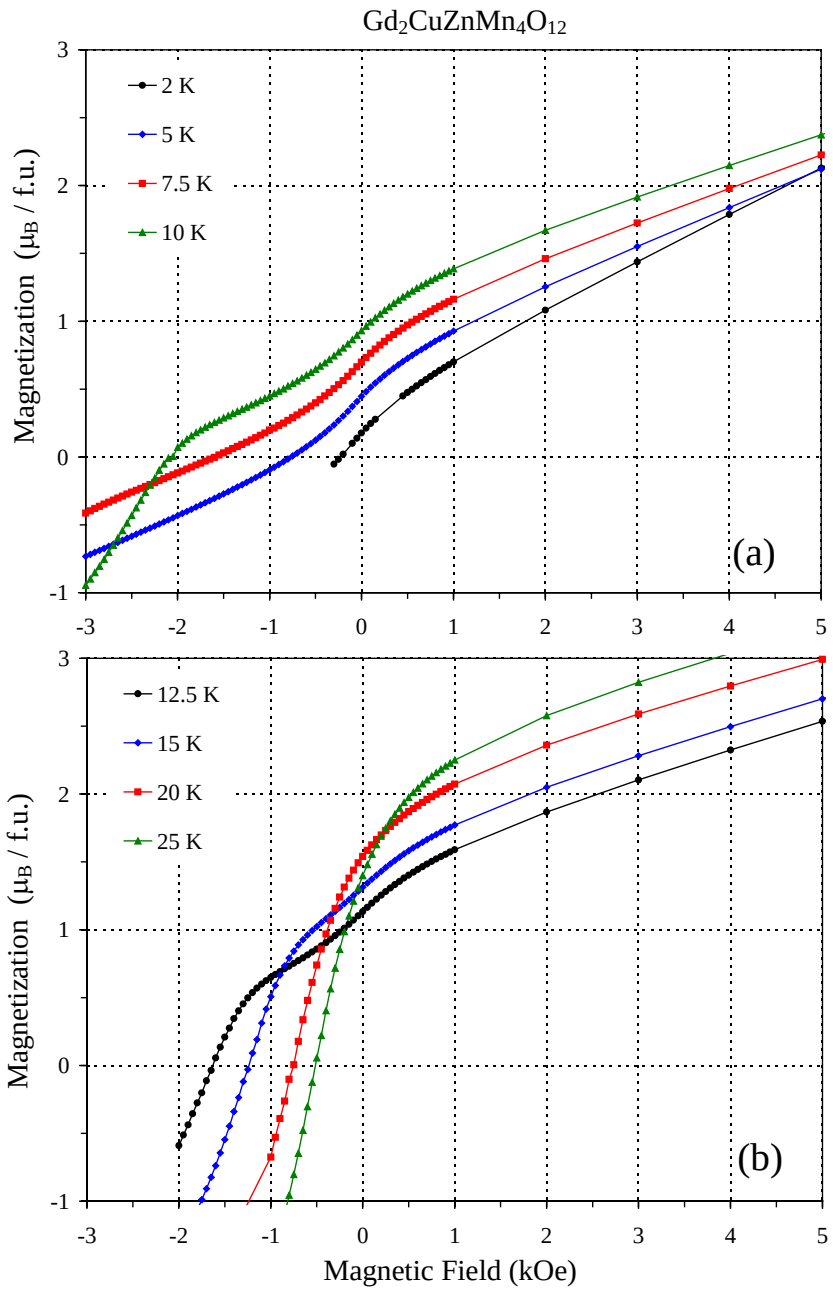

Figure S5a, 5b. *M* versus *H* curves of $Gd_2CuZnMn_4O_{12}$ in the vicinity of origin at different temperatures. These curves were used for plotting Figure 10 in the main text.

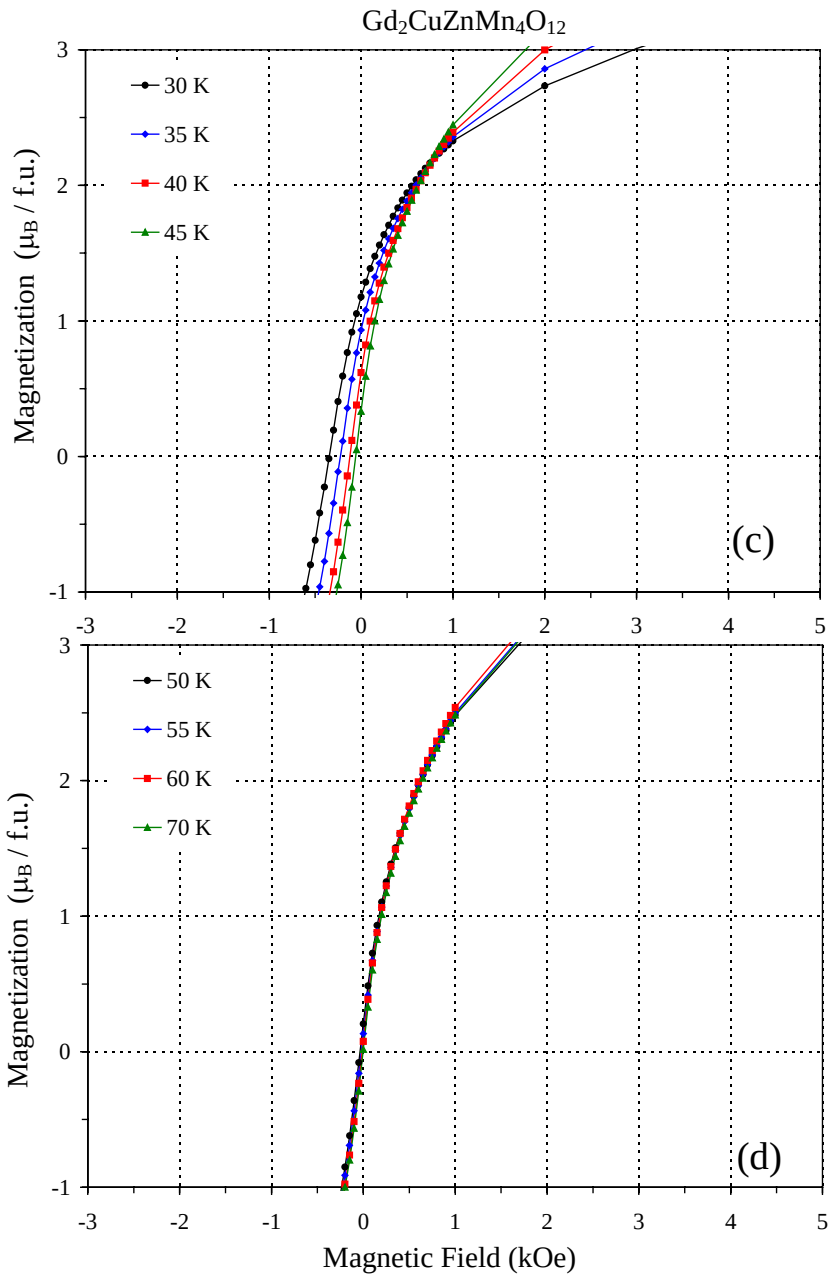

Figure S5c, 5d. *M* versus *H* curves of $Gd_2CuZnMn_4O_{12}$ in the vicinity of origin at different temperatures. These curves were used for plotting Figure 10 in the main text.

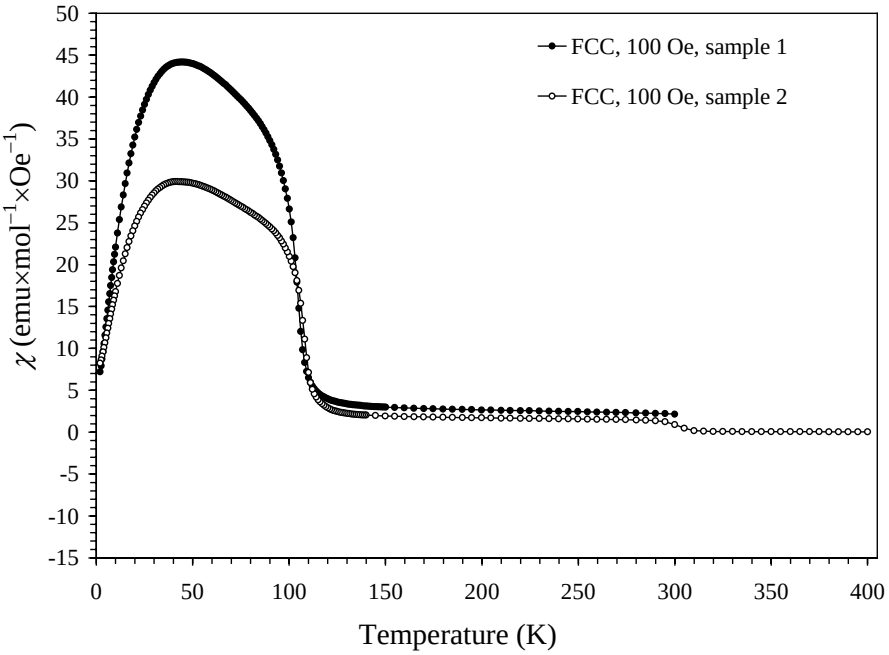

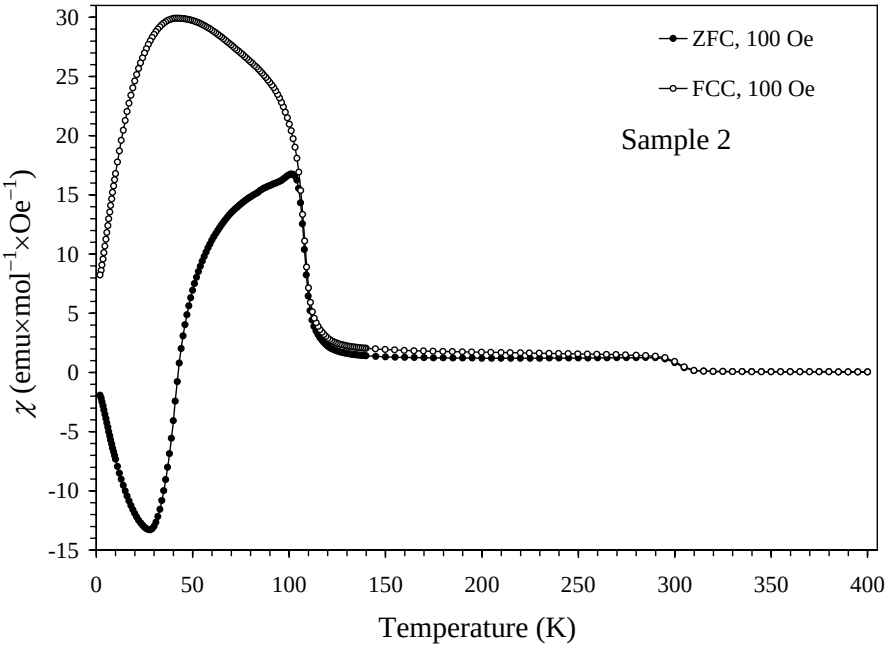

Figure S6a. Comparison of magnetic properties of the $Gd_2CuZnMn_4O_{12}$ samples prepared at 6GPa and at 1500 K for 2 h in an Au capsule (sample 1) and at 6 GPa and at 1730 K for 2 h in a Pt capsule (sample 2). Negative values on the ZFC curve for sample 2 could be caused by a negative initial trapped field inside a magnetometer (the magnet-reset option did not work during the measurement of sample 2, while the magnet-reset option was applied during the measurement of sample 1 (for the ZFC curve)).

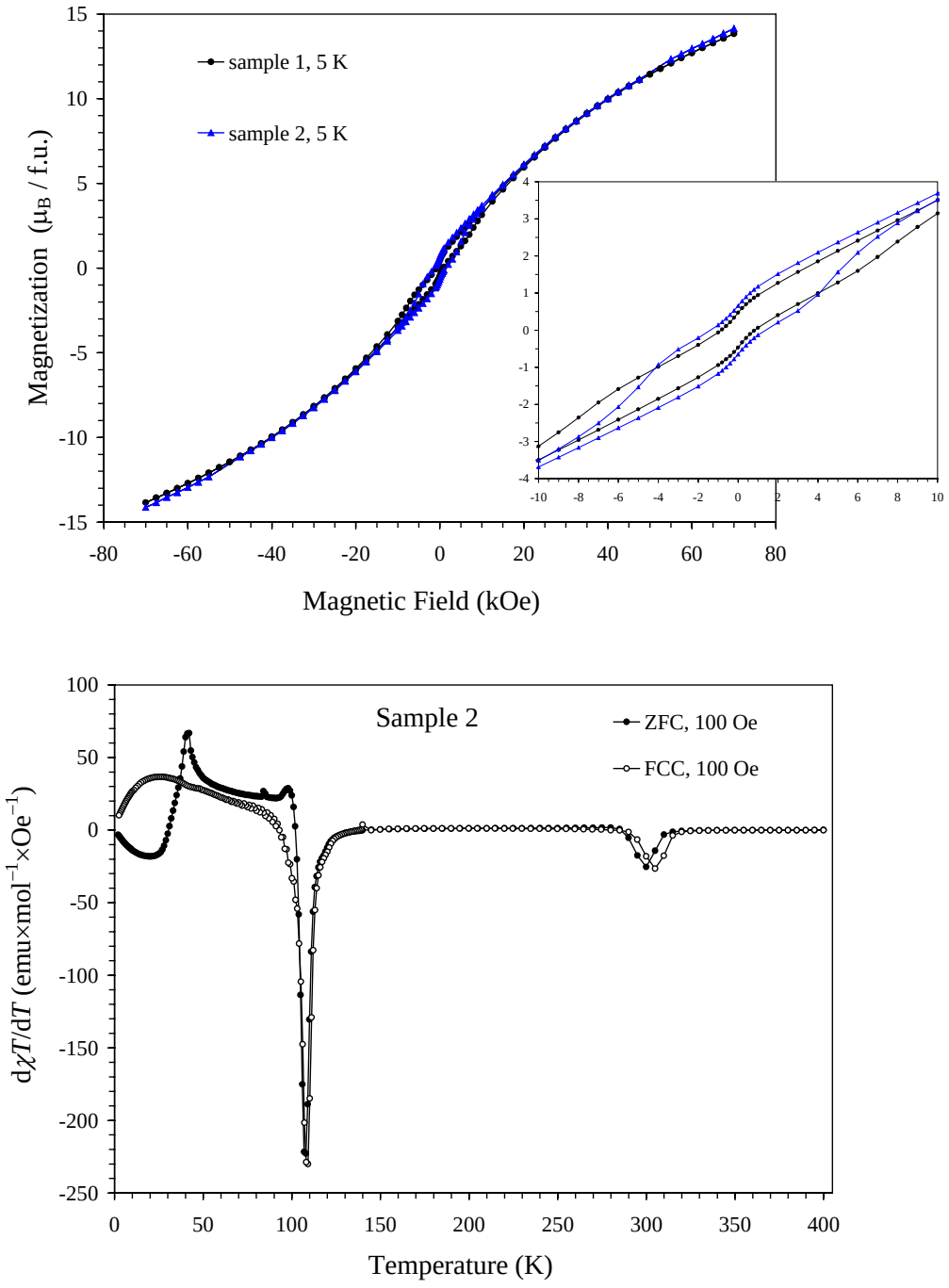

Figure S6b. Comparison of magnetic properties of the $Gd_2CuZnMn_4O_{12}$ samples prepared at 6GPa and at 1500 K for 2 h in an Au capsule (sample 1) and at 6 GPa and at 1730 K for 2 h in a Pt capsule (sample 2).